Novel piezoelectric actuation mechanism for a gimbal-less mirror in 2D raster scanning applications

2011 J. Micromech. Microeng. 21 075001

(http://iopscience.iop.org/0960-1317/21/7/075001)

J. Micromech. Microeng. **21** (2011) 075001 (9pp) doi:10.1088/0960-1317/21/7/075001

Novel piezoelectric actuation mechanism for a gimbal-less mirror in 2D raster scanning applications

Kah How Koh[1], Takeshi Kobayashi[2], Jin Xie[3], Aibin Yu[4] and Chengkuo Lee[1,5]

[1] Department of Electrical & Computer Engineering, National University of Singapore, 4 Engineering Drive 3, Singapore 117576
[2] National Institute of Advanced Industrial Science and Technology (AIST), 1-2-1 Namiki, Tsukuba, Ibaraki 305-8564, Japan
[3] Institute of Microelectronics (IME), Agency for Science, Technology and Research (A*STAR), 11 Science Park Road, Singapore 117685
[4] Micron Semiconductor Asia Pte Ltd, 990 Bendemeer Road, Singapore 339942

E-mail: elelc@nus.edu.sg

Received 22 August 2010, in final form 14 April 2011
Published 1 June 2011
Online at stacks.iop.org/JMM/21/075001

Abstract
In this paper, we present the design, fabrication and measurement results of a 2D scanning mirror actuated by 1 × 10 piezoelectric $Pb(Zr,Ti)O_3$ (PZT) cantilever actuators integrated on a thin silicon beam. A combination of bulk silicon micromachining based on a silicon-on-insulator (SOI) substrate and thin-film surface micromachining on a 5 μm thick Si device layer is used to fabricate the device. Multi-layers of Pt/Ti/PZT/Pt/Ti are deposited as electrode materials. A large silicon mirror plate (5 mm × 5 mm) and a 1 × 10 PZT cantilever array arranged in parallel are formed after the backside release process. The ten PZT cantilever actuators are electrically isolated from one another. The device can operate in three modes: bending, torsional and mixed (or combinational) modes. In bending mode, the first resonant frequency was measured to be 30 Hz and an optical deflection angle of ±8° was obtained when all ten cantilevers were actuated at 9 V_{pp}. In torsional mode, the resonant frequency was measured to be 89 Hz and an optical deflection angle of ±4.6° was obtained by applying a gradually declining ac voltage started at 8 V_{pp} to two sets of actuators, where each set comprises five cantilever actuators of the said 1 × 10 array, i.e. 1–5 and 6–10. A 2D raster scanning pattern was achieved in the mixed mode when the bending mode was carried out by cantilever actuators of 4–7 and the torsional modes were exercised by two different sets of cantilever actuators, i.e. 1–3 and 8–10, under opposite biasing direction. This mixed mode operation mechanism demonstrates the first 2D raster scanning mirror-driven beam actuators.

(Some figures in this article are in colour only in the electronic version)

1. Introduction

Micro-opto-electro-mechanical systems (MOEMS) have been promising candidates in a wide variety of applications. These include various modules deployed in fiber optic communication networks such as tunable lasers [1], optical switches [2–5], variable optical attenuators [6–10], reconfigurable add/drop multiplexers [11]. In addition, MOEMS devices have also been conceptualized for a large range of image display applications such as projection displays [12–14], biomedical imaging [15, 16] and retinal scanning [17, 18]. In recent years, micro-electro-mechanical systems (MEMS) display have formed a circle of growing interest, with the development of handheld pico-projectors based on

[5] Author to whom any correspondence should be addressed.

scanning mirror technology becoming an intriguing killer application in consumer electronics, game consoles and automobiles [13, 19]. The most well known commercial product is probably the digital micromirror device (DMD), which is the core of digital light processing (DLP) projection technology developed by Texas Instrument in 1987 [20]. In 1994, Solgaard *et al* developed the grating light valve (GLV) technology, providing an alternative technology for implementation in commercial projectors [21].

Several research groups have successfully demonstrated scanning micromirrors using various actuation mechanisms, including electrostatic [22–27], electromagnetic [28–31], electrothermal [32–35] and piezoelectric [36–38] approaches. To achieve large mechanical rotation angles, gimbaled mirrors using torsion springs are the popular design for integration with the various actuation mechanisms. A gimbaled two-dimensional (2D) mirror [22–29, 35–38] normally consists of two independent rotational axes placed orthogonally to each other, allowing mechanical decoupling of the rotation of two axes and elimination of crosstalk of both drive signals. However, such a gimbaled design often requires a large portion of the die area to accommodate such structures, e.g. inner and outer frames needed for 2D scanning. In contrast, gimbal-less 2D mirrors [30, 32–34] realize two-axis scanning while offering advantages of single mirror and smaller footprint for the same mirror size. The tradeoff, however, lies in the dependence of the deflection of the mirror plate on the mechanical action of all the actuators and the biasing scheme used to drive the actuators.

By having a mirror at the free end of a cantilever, Isikman *et al* demonstrated 2D scanning patterns by using two sets of ac signals to oscillate this mirror which is coated with a NiFe soft magnetic film at a fundamental mode frequency (bending mode) and second mode frequency (torsional mode) [30]. Jia *et al* also reported a gimbal-less electrothermal tip-tilt-piston mirror based on folded dual S-shaped bimorphs [32]. In this design, the dual S-shaped bimorph actuators are connected to the mirror plate by pure SiO_2 joints, and this unique design allows for no lateral shift and rotation-axis shift for piston and rotation scanning respectively. In another similar design by Xu *et al*, a circular single-crystal silicon mirror plate actuated by a folded curved thermal bimorph actuator was fabricated [33]. The mirror plate was connected to the bimorphs by flexural springs, making the device capable of 3-DOF actuation. A more straightforward and compact design was demonstrated by Schweizer *et al* [34]. In this work, the two orthogonal angular motions were given by the same 'L'-shaped thermal bimorph cantilever beam, allowing 2D scanning to be made possible by the simultaneous thermomechanical excitation of the cantilever.

A gimbal-less mirror for 2D scanning has also been realized by piezoelectric bending mode and torsional mode. This is illustrated in our previous reported research attempt, where a silicon micromirror driven by 1 × 10 piezoelectric $Pb(Zr,Ti)O_3$ beam actuators was fabricated and characterized [39]. In our previous work, we designed ten PZT actuators to be electrically connected in series and 2D Lissajous scan patterns are obtained by one-half of the actuators at a resonant frequency corresponding to bending mode while the remaining other half of the actuators at a resonant frequency corresponding to torsional mode. As such, the mirror in our previous work achieved torsional scanning solely by resonance phenomenon.

In this paper, a novel piezoelectric-driven scanning mirror using a mechanical supporting beam integrated with a 1 × 10 PZT cantilever array is explored and characterized. This design is similar to that in [39], except that the electrical connections to each of the cantilevers are now separated, hence allowing the cantilevers' actuation behavior to be individually manipulated. More importantly, with the separated electrical connections, we can now achieve torsional scanning based on the difference in the ac biasing voltage applied to the ten piezoelectric cantilevers. This actuation mechanism differs greatly from that in [39] and the actuation mechanisms of gimbaled mirror in torsional mode, i.e. the mirror rotation is generated against the torsion spring or torsion bar. As such, besides depending on the resonance phenomenon for torsional scanning, the difference in the direction of cantilever displacement due to the 180° phase difference in the applied bias also helps to magnify the torsional scanning of the mirror. Although thermal bimorph beam actuators have been well characterized in terms of their capability of generating large deflection, i.e. in bending mode, no design of torsional mirror driven by beam actuators has been reported in thermal actuation and piezoelectric actuation schemes yet. As such, our unique design of piezoelectric cantilever beam actuator is the first demonstration of a large torsion mirror using a beam actuator.

2. Design, modeling and fabrication

A schematic diagram of the PZT MEMS scanning mirror demonstrated in this paper is shown in figure 1. A silicon mirror plate (5 mm long × 5 mm wide × 0.4 mm thick) and a mechanical supporting beam (3 mm long × 5 mm wide × 5 μm thick) integrated with 1 × 10 arrayed PZT cantilever actuators (3 mm long × 0.24 mm wide × 5 μm thick for each cantilever) are arranged in parallel along the longitudinal direction of the cantilevers. The electrical connections to each cantilever are separated from one another, with individual bonding pads connected to each of the top and bottom electrodes of the cantilevers.

The micromirror can be actuated in three modes: bending, torsional and mixed (or combinational). To elicit bending mode, an ac driving voltage is applied simultaneously to all ten cantilevers. The displacement introduced by the bent cantilevers under bias causes the mirror to undergo translational and rotational movements about the y-axis, hence achieving horizontal scanning effect when a laser is shone on the mirror surface. The inset in figure 1 illustrates the device in torsional mode, where, for example, cantilevers 1–5 are biased in such a way that they bend downward while cantilevers 6–10 are biased to bend upward in the opposite direction. This difference in the bending direction for the two sets of actuators causes the mirror to rotate about the x-axis, achieving vertical scanning effect when ac voltages of varying V_{pp} are applied to

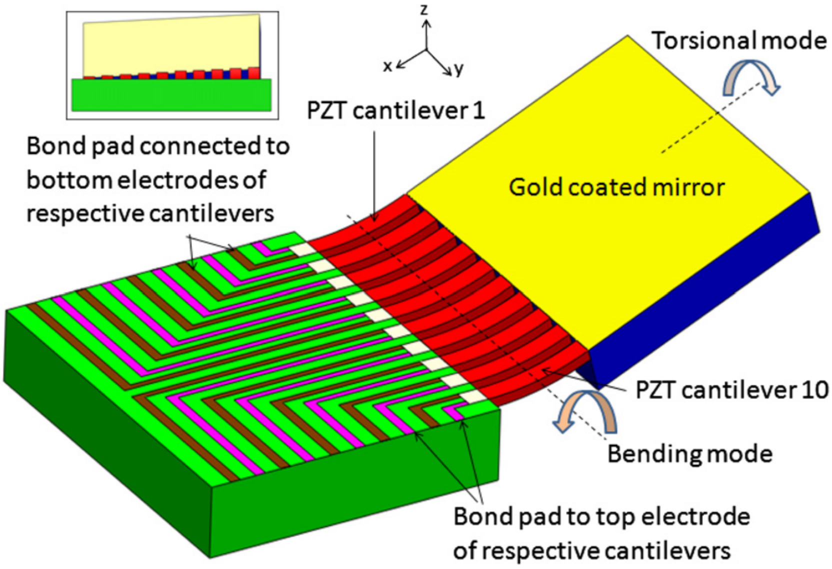

Figure 1. Schematic diagram of a PZT 2D scanning mirror where it twists or bends when different ac voltage combinations are applied separately to the ten cantilevers. The inset shows torsional mode where a set of five cantilevers 1–5 bend in one direction, while the other set of five cantilevers 6–10 bend in the opposite direction.

the ten cantilevers. To obtain a 2D scan with two orthogonal scan axes, i.e. mixed mode, the ten cantilevers are biased such that both bending and torsional modes occur simultaneously, causing the mirror plate to rotate about the x- and y-axes at the same time. The details of the biasing configuration to elicit a 2D scan will be described in the later part of the paper.

Modal analysis by finite element software ABAQUS is done to explore the phenomenon of bending and torsional rotations at different harmonic frequencies. Simulation results have demonstrated that our 1×10 array of cantilevers and mirror design are able to have multiple resonant modes with all six degrees of freedom in three-dimensional space. The mode shape in figure 2, with a calculated modal frequency of 93 Hz, is the first torsional mode derived from ABAQUS simulation.

To evaluate the mechanical deflection angle under a dc condition, a mathematical model is necessary to compute the effect of the dc bias on the deflection angle under both bending and torsional modes. The displacement of the cantilever is related to the dc bias by the following equations [40]:

$$\delta_{\text{cantilever}} = \frac{3AB}{K}(L_{\text{cantilever}})^2 V \ \ d_{31} \tag{1}$$

$$A = S_{\text{si}} S_{\text{PZT}} (S_{\text{PZT}} t_{\text{Si}} + S_{\text{Si}} t_{\text{PZT}}) \tag{2}$$

$$B = \frac{t_{\text{Si}}(t_{\text{Si}} + t_{\text{PZT}})}{S_{\text{PZT}} t_{\text{Si}} + S_{\text{Si}} t_{\text{PZT}}} \tag{3}$$

$$\begin{aligned} K = {} & (S_{\text{Si}})^2 (t_{\text{PZT}})^4 + 4 S_{\text{Si}} S_{\text{PZT}} t_{\text{Si}} (t_{\text{PZT}})^3 + 6 S_{\text{Si}} S_{\text{PZT}} (t_{\text{Si}})^2 (t_{\text{PZT}})^2 \\ & + 4 S_{\text{Si}} S_{\text{PZT}} (t_{\text{Si}})^3 (t_{\text{PZT}}) + (S_{\text{PZT}})^2 (t_{\text{Si}})^4, \end{aligned} \tag{4}$$

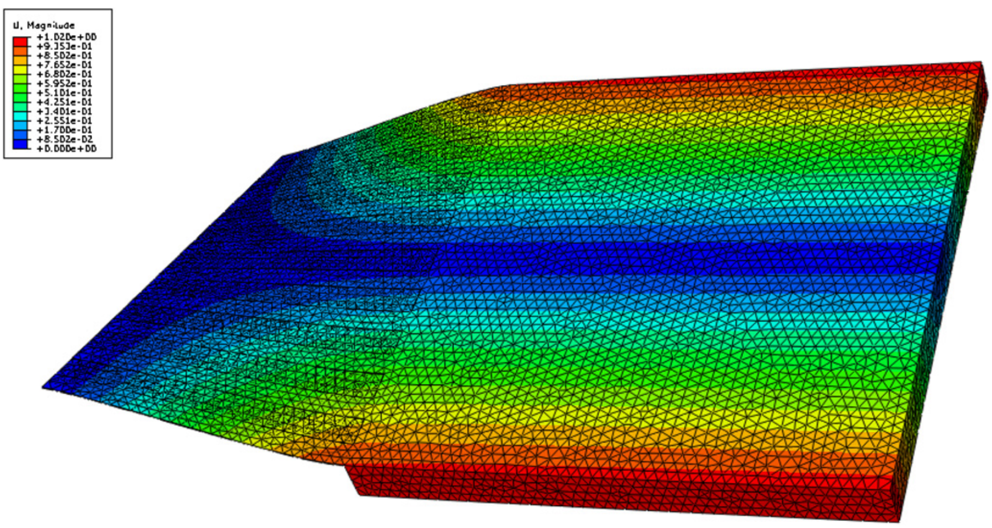

Figure 2. Modal analysis of the scanning mirror using ABAQUS, showing the second mode: torsional mode at 93 Hz.

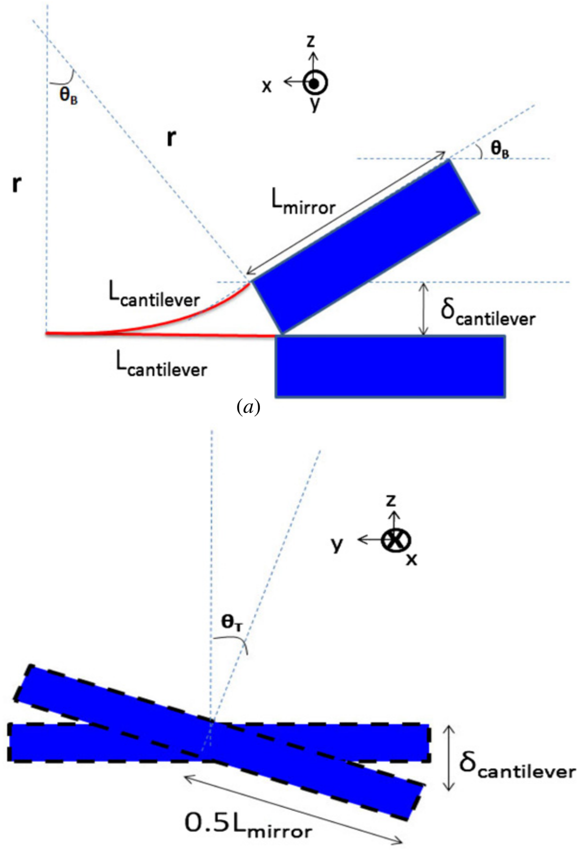

Figure 3. Schematic drawing of the biased PZT cantilever with a mirror plate during (*a*) bending mode, with a vertical displacement of $\delta_{\mathrm{cantilever}}$ and mechanical rotation angle of θ_B; (*b*) torsional mode, with a vertical displacement of $\delta_{\mathrm{cantilever}}$ and mechanical rotation angle of θ_T.

where δ is the displacement of the actuator, $L_{\mathrm{cantilever}}$ is the length of the cantilever (3 mm), V is the applied voltage, S_{si} and S_{PZT} are the compliances of the structural Si layer (6.0×10^{-12} Pa^{-1}) and PZT thin film (1.43×10^{-11} Pa^{-1}) respectively, t_{Si} and t_{PZT} are the respective thicknesses of the structural silicon (5 μm) and PZT film (3 μm). The transverse piezoelectric constant, d_{31}, may be assumed to be -100 pm V^{-1} when calculating the theoretical actuated displacement caused by the piezoelectric effect.

Figure 3(*a*) relates the displacement of the cantilever to the mechanical deflection angle of the mirror during bending mode. Equation (5) can be derived from figure 3(*a*):

$$\delta_{\mathrm{cantilever}} = r - r\cos\theta_B, \tag{5}$$

where $\delta_{\mathrm{cantilever}}$ is the vertical displacement of the cantilever tip, r is the radius of curvature, θ_B is the mechanical deflection angle experienced by the cantilever under bias during bending mode. Assuming that θ_B is small, by small angle approximation,

$$\cos\theta_B = 1 - \tfrac{1}{2}\theta_B^2 \tag{6}$$

$$r = \frac{L_{\mathrm{cantilever}}}{\theta_B}. \tag{7}$$

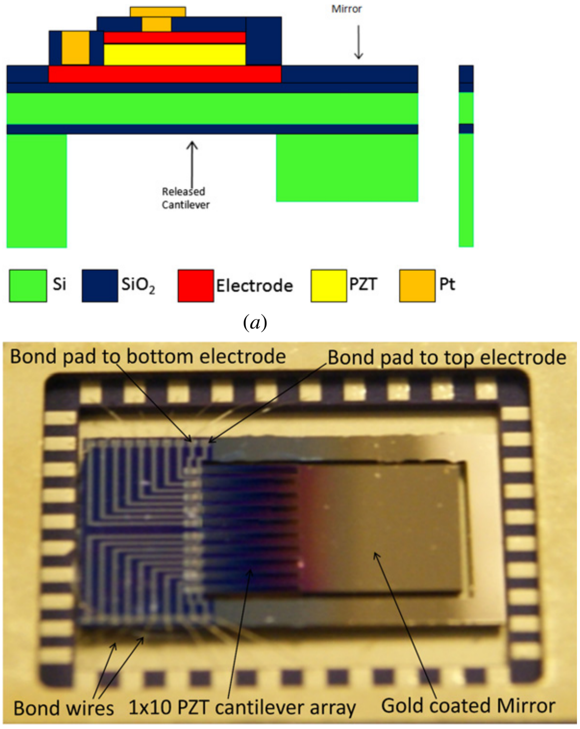

Figure 4. (*a*) Schematic diagram illustrating the cross section of the device after the microfabrication of PZT cantilever actuators and mirror. (*b*) A magnified photo showing the packaged device with a gold-coated mirror surface. The bond pads are connected to the package via gold bond wires.

Substituting equations (1), (6) and (7) into (5) and making θ_B the subject,

$$\theta_B = \frac{6ABL_{\mathrm{cantilever}}V\ d_{31}}{K}. \tag{8}$$

On the other hand, figure 3(*b*) is used to derive the relationship between the displacements of the cantilever and the mechanical deflection angle of the mirror during torsional mode:

$$\sin\theta_T = \frac{\delta_{\mathrm{cantilever}}}{0.5L_{\mathrm{mirror}}}, \tag{9}$$

where $\delta_{\mathrm{cantilever}}$ is the vertical displacement of the cantilever tip, L_{mirror} is the length of the mirror, θ_T is the mechanical deflection angle experienced by the cantilever under bias during torsional mode. Substituting equations (1) into (9) and making θ_T the subject,

$$\theta_T = \sin^{-1}\left(\frac{6ABL_{\mathrm{cantilever}}^2V\ d_{31}}{KL_{\mathrm{mirror}}}\right). \tag{10}$$

Hence, from this mathematical analysis, the derived equations (8) and (10) can be used to understand how a change in the dc bias affects the mechanical rotation angle during bending and torsional modes respectively.

Figure 4(*a*) shows the schematic cross-sectional drawing of the PZT cantilever actuators and mirror after microfabrication. The device is micromachined from a silicon-on-insulator (SOI) substrate of a 5 μm thick Si device layer,

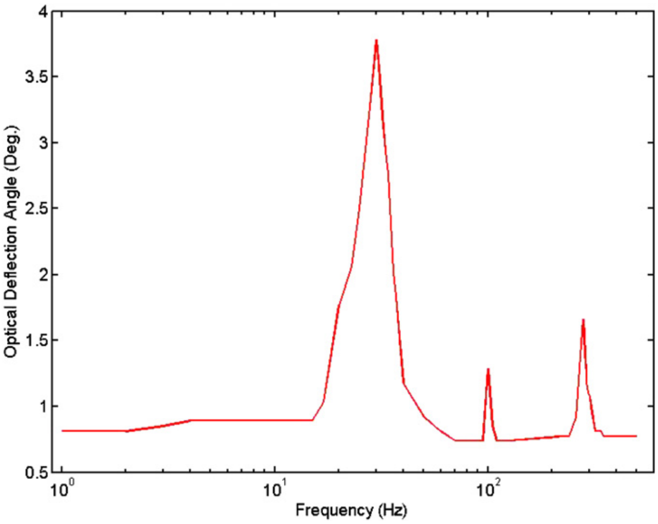

Figure 5. Frequency response measured for bending mode when a sinusoidal ac voltage of 5 V_{pp} was applied to all ten PZT cantilevers simultaneously.

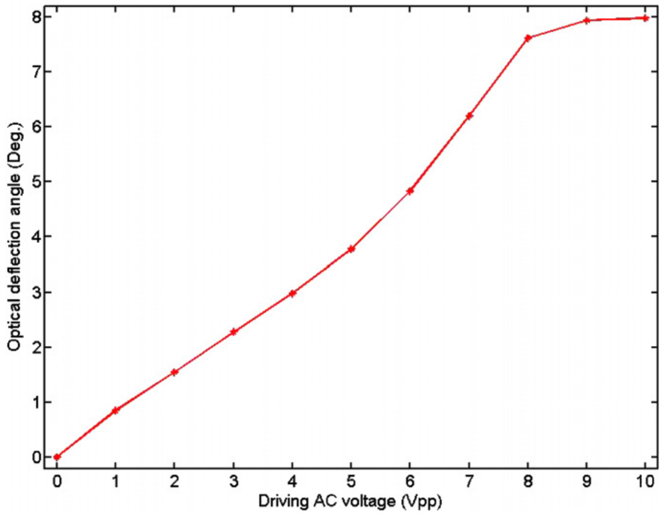

Figure 6. Measured ODA versus peak-to-peak ac driving voltage applied to all ten PZT cantilevers simultaneously during the resonance condition at 30 Hz.

with multi-layers of Ti/Pt/$LaNiO_3$/PZT/$LaNiO_3$/Ti/Pt deposited as electrode materials. The details of the fabrication process for this device can be obtained from [40, 41]. To compensate for the possible increase in dynamic deformation due to a large scanning angle and frequency, a thick Si substrate is left beneath the mirror surface to maintain the mirror flatness and rigidity. A thin film of gold was sputtered on the mirror surface using a shadow mask. This is to improve the reflectivity of the mirror surface.

After the fabrication process, the device is assembled on a dual in-line package (DIP) and the bond pads were connected by gold bond wires to the metal pins of the DIP as shown in figure 4(*b*). To enhance the piezoelectric characteristics of the device, poling treatment is conducted on the PZT thin film actuators at room temperature. A dc voltage of 30 V, which is equivalent to a polarization electric field of 100 kV cm^{-1}, was applied to each of the PZT thin film actuators for 5 min, with the poling direction from the bottom electrode to the top electrode.

3. Results and discussion

3.1. Bending mode

In the bending mode operation of the PZT scanning mirror, the sinusoidal ac driving voltage was applied simultaneously to all the top electrodes of the cantilevers, while the bottom electrodes of all the cantilevers were grounded. An He/Ne laser of wavelength 632.8 nm was shone on the mirror surface, forming a horizontal scan line trajectory on the screen. Optical deflection angles at different frequencies of the ac signal were calculated using the horizontal scanned beam length and the distance between the mircromirror and the screen. The frequency response for bending mode is shown in figure 5. An optical deflection angle (ODA) of $\pm 3.8^\circ$ was obtained at 30 Hz when 5 V_{pp} was applied to all ten PZT cantilevers simultaneously. This resonance frequency corresponds closely to the first modal frequency of 31 Hz simulated by ABAQUS. Figure 6 shows the measured ODA for various V_{pp} applied to the ten cantilevers during the resonance condition at 30 Hz. The ODA increases rather linearly with increasing ac driving voltage, reaching saturation for voltages above 8 V_{pp}. An ODA of $\pm 8^\circ$ was obtained when an ac voltage of 10 V_{pp} was applied. The saturation behavior at an ODA of $\pm 8^\circ$ is due to the mirror plate coming into contact with the bottom of the package during the scanning operation, causing the mirror oscillation at resonance to be damped and limited. The distance between the mirror plate and the base of the DIP has been determined to be 500 μm using an optical microscope.

3.2. Torsional mode

Figure 7(*a*) illustrates the biasing configuration for torsional mode operation. A potential divider was implemented to split the function generator ac output into five equal potentials at the potential nodes between each resistor. The potential divider was realized by using five equal resistors of resistance 20 Ω each connected in series. For the set of cantilevers 1–5, the top electrodes for these cantilevers were connected to the various potential nodes, while the bottom electrodes of these cantilevers were grounded. The reverse setup was made for the set of cantilevers 6–10, i.e. the top electrodes for these cantilevers were grounded while the bottom electrodes were connected to the various potential nodes. As a result, each cantilever will have a different ac bias amplitude as evident from the look-up table in figure 7(*b*). The results show the largest and the smallest cantilever displacements which are introduced at the mirror edges and center respectively. More importantly, the generated displacements for the two sets of cantilevers are toward opposite directions, resulting in torsional deflection of the mirror plate.

(*a*)

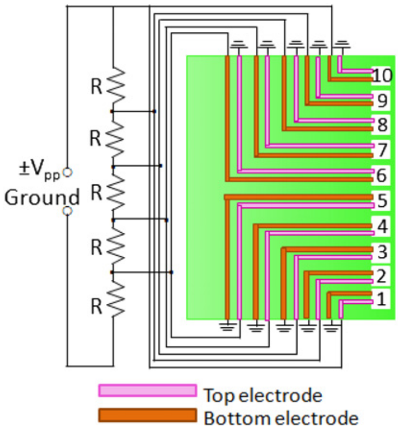

(*b*)

Actuators	Relative bias of top to bottom electrode /V	
Vpp of function generator	5V	10V
1	5.00	10.00
2	4.00	8.00
3	3.00	6.00
4	2.00	4.00
5	1.00	2.00
6	-1.00	-2.00
7	-2.00	-4.00
8	-3.00	-6.00
9	-4.00	-8.00
10	-5.00	-10.00

Figure 7. (*a*) Schematic drawing illustrating the electrical connections of the top and bottom electrodes of each cantilever to the function generator for torsional mode operation. (*b*) A look-up table illustrating the individual V_{pp} bias driving each cantilever for the bias setup shown in (*a*).

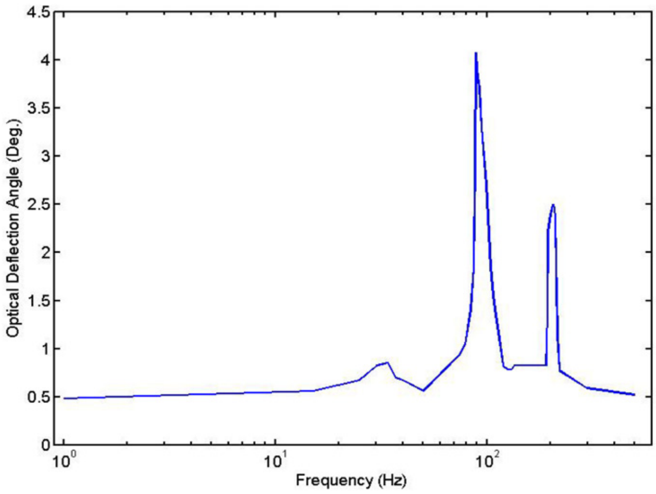

Figure 8. Frequency response measured for torsional mode when a sinusoidal ac voltage of 5 V_{pp} is applied by the function generator.

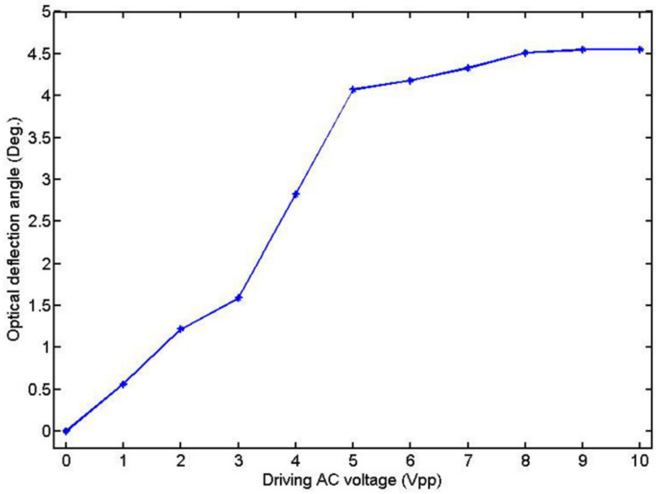

Figure 9. Measured ODA versus peak-to-peak ac driving voltage applied by the function generator during torsional mode.

The frequency response for torsional mode is shown in figure 8. An ODA of ±4° was obtained when an ac voltage of 5 V_{pp} at 89 Hz was applied by the function generator. This resonant frequency obtained for the experimentally tested device corresponds closely to the simulated modal frequency of 93 Hz obtained by ABAQUS.

Figure 9 shows the measured ODA for various V_{pp} applied by the function generator during the resonance condition at 89 Hz. An ODA of ±4.5° was obtained when an ac voltage of 10 V_{pp} was applied. The observed saturation behavior above 7 V_{pp} may suggest that the ODA of ±4.5° is the largest that can be achieved by the device in torsional mode operation, i.e. the torsional mechanical supporting beam has reached its actuation limitation. In addition, for the same V_{pp}, a larger ODA is obtained during bending mode, compared to torsional mode. This is because of the larger torsional stiffness of the cantilever beam actuators as compared to their bending stiffness. Moreover, the V_{pp} from the function generator was simultaneously directly applied to all ten cantilever actuators in bending mode, while in torsional mode, the V_{pp} of the function generator was applied only to cantilevers 1 and 10, and the rest of the cantilever actuators 2–5 and 9–6 were biased at a V_{pp} value gradually reduced and lower than that of the generator.

3.3. Mixed mode

In mixed (or combinational) mode operation, bending and torsional actuations occur simultaneously to produce a 2D Lissajous scanning pattern. Two functional generators were used separately to bias cantilevers 4–7 at bending mode and cantilevers 1–3 and 8–10 at torsional mode, respectively. As shown in figure 10(*a*), the sinusoidal ac driving voltage of 30 Hz from the first function generator, $V_{1,pp}$, was applied simultaneously to all the top electrodes of the cantilevers 4–7, while the bottom electrodes of the cantilevers were grounded.

(*a*)

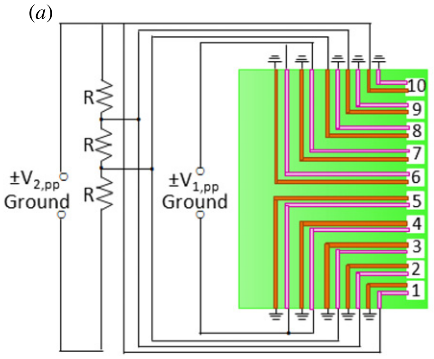

(*b*)

	Relative bias of top to bottom electrode /V			
Vpp of Function generator	V1 = 5V	V2 = 5V	V1 = 10V	V2 = 10V
Bias configuration	4-7	1-3,8-10	4-7	1-3,8-10
1	-	5.00	-	10.00
2	-	3.33	-	6.67
3	-	1.67	-	3.33
4	5.00	-	10.00	-
5	5.00	-	10.00	-
6	5.00	-	10.00	-
7	5.00	-	10.00	-
8	-	-1.67	-	-3.33
9	-	-3.33	-	-6.67
10	-	-5.00	-	-10.00

Figure 10. (*a*) Schematic drawing illustrating the electrical connections of the top and bottom electrodes of each cantilever to the two function generators for mixed mode operation. (*b*) A look-up table illustrating the individual V_{pp} bias driving each cantilever for the bias setup shown in (*a*).

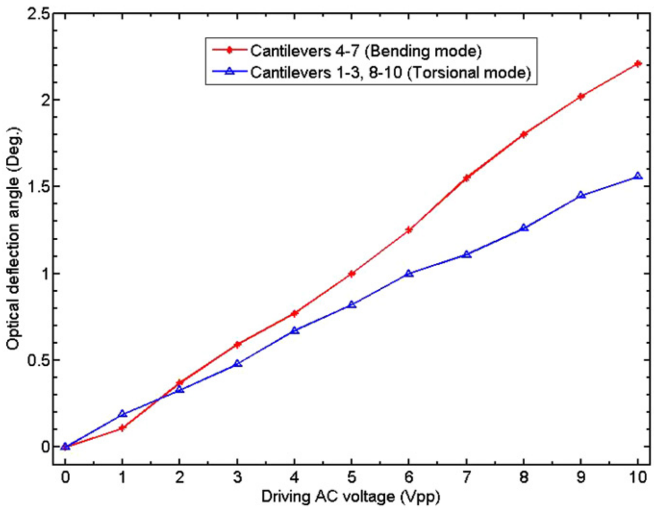

Figure 11. Measured ODA versus peak-to-peak ac driving voltage applied to the ten PZT cantilevers. Cantilevers 4–7 were operated in bending mode and biased by the function generator $V_{1,\mathrm{pp}}$. Cantilevers 1–3 and 8–10 were operated in torsional mode and biased by the function generator $V_{2,\mathrm{pp}}$.

The ac output of 89 Hz from the second function generator, $V_{2,\mathrm{pp}}$, was split by a potential divider into three equal potentials at the potential nodes between each resistor. For the set of cantilevers 1–3, the top electrodes for these cantilevers were connected to the various potential nodes, while the bottom electrodes of these cantilevers were grounded. The reverse setup is made for the set of cantilevers 8–10. As a result, the generated displacement for the cantilevers 1–3 and 8–10 is in opposite directions, resulting in torsional rotation of the mirror plate. The look-up table in figure 10(*b*) indicates the individual V_{pp} bias driving each cantilever for the bias setup for mixed mode operation.

Figure 11 shows the measured ODA obtained under various ac driving voltages for the two sets of cantilevers 4–7 and 1–3, 8–10 operating in bending and torsional actuations respectively. An ODA of $\pm 2.2°$ was obtained when 10 $\mathrm{V_{pp}}$ was applied to cantilevers 4–7 for bending actuation. This value obtained is much smaller when compared to that of $\pm 8°$ obtained when all ten cantilevers were biased at 10 $\mathrm{V_{pp}}$. This decrease in ODA is expected as the number of cantilevers involved in actuating the mirror is lowered from 10 to 4. In torsional actuation, an ODA of $\pm 1.55°$ was obtained when 10 $\mathrm{V_{pp}}$ was applied by the second function generator.

2D scans using this device were demonstrated by adopting the bias configuration shown in figure 10(*a*). Figure 12(*a*) shows the Lissajous scan pattern obtained in resonance mixed mode operation, with $V_1 = 5$ $\mathrm{V_{pp}}$ at 30 Hz and $V_2 = 5$ $\mathrm{V_{pp}}$ at 89 Hz. Figure 12(*b*) shows a Lissajous scan pattern with a larger horizontal scanning trajectory. This is due to a higher biasing voltage V_1, i.e. 10 $\mathrm{V_{pp}}$, applied to elicit bending actuation.

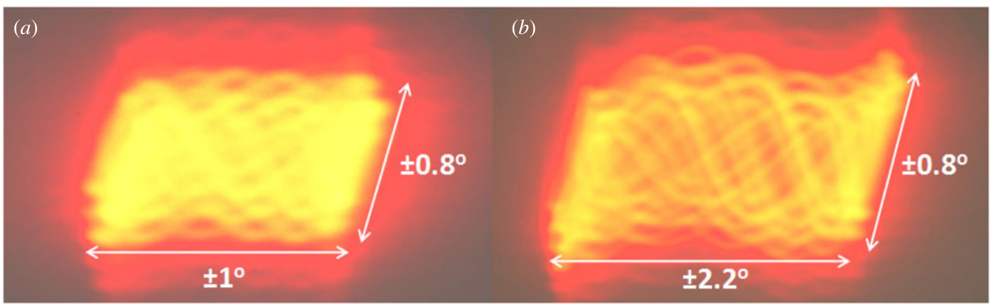

Figure 12. Lissajous scan pattern obtained in resonance of mixed mode operation, with (*a*) $V_1 = 5$ $\mathrm{V_{pp}}$, 30 Hz and $V_2 = 5$ $\mathrm{V_{pp}}$, 89 Hz. Horizontal and vertical scanning angles of 1° and 0.8° are obtained respectively. (*b*) $V_1 = 10$ $\mathrm{V_{pp}}$, 30 Hz and $\mathrm{V_2} = 5$ $\mathrm{V_{pp}}$, 89 Hz. Horizontal and vertical scanning angles of 2.2° and 0.8° are obtained respectively.

4. Conclusions

A novel piezoelectric-driven 2D scanning micromirror using a mechanical supporting beam integrated with 1×10 PZT cantilever actuators has successfully been designed, fabricated and tested. Three modes of scanning operation have been investigated: bending, torsional and mixed. By applying 8 and 5 V_{pp}, the mirror can achieve a horizontal and vertical resonant optical scan range of $\pm 7.8°$ and $\pm 4.2°$ in the bending and torsional modes respectively. In mixed mode operation, a resonant optical scan range of $\pm 2.2°$ and $\pm 0.8°$ was obtained for bending and torsional actuations respectively. Clear 2D scanning Lissajous patterns were also obtained successfully in mixed mode operation. These raster scanning images demonstrate the potential of the device in imaging applications and will be explored in the near future.

Acknowledgments

The authors would like to acknowledge the financial contributions from University Research Fund under grant no R-263-000-475-112 and Academic Research Fund under grant no R-263-000-598-112 at the National University of Singapore, Singapore, and the PhD scholarship grant received from GLOBALFOUNDRIES Singapore.

References

[1] Liu A Q and Zhang X M 2007 A review of MEMS external cavity *J. Micromech. Microeng.* **17** R1–13
[2] Lee C and Wu C-Y 2005 Study of electrothermal V-beam actuators and latched mechanism for optical switch *J. Micromech. Microeng.* **15** 11–9
[3] Chen W-C, Lee C, Wu C-Y and Fang W 2005 A new latched 2 × 2 optical switch using bi-directional movable electrothermal H-beam actuators *Sensors Actuators* A **123–124** 563–9
[4] Wu M C, Solgaard O and Ford J E 2006 Optical MEMS for lightwave communication *J. Lightwave Technol.* **24** 4433–54
[5] Liao B-T, Shen H-H, Liao H-H and Yang Y-J 2009 A bi-stable 2 × 2 optical switch monolithically integrated with variable optical attenuators *Opt. Express* **17** 19919–25
[6] Koh K H, Lee C and Kobayashi T 2010 A piezoelectric-driven three-dimensional MEMS VOA using attenuation mechanism with combination of rotational and translational effects *J. Microelectromech. Syst.* **18** 1370–9
[7] Koh K H, Lee C and Kobayashi T 2010 Low-voltage driven MEMS VOA using attenuation mechanism based on piezoelectric beam actuators *IEEE Photonics Lett.* **22** 1355–7
[8] Lee C and Yeh J A 2008 Development and evolution of MOEMS technology in variable optical attenuators *J. Micro/Nanolith. MEMS MOEMS* **7** 021003
[9] Lee C, Hsiao F-L, Kobayashi T, Koh K H, Ramana P V, Xiang W, Yang B, Tan C W and Pinjala D 2009 A 1-V operated MEMS variable optical attenuator using piezoelectric PZT thin film actuators *IEEE J. Sel. Top. Quantum Electron.* **15** 1529–36
[10] Lee C 2007 A MEMS VOA using electrothermal actuators *J. Lightwave Technol.* **25** 490–8
[11] Antoine C, Li X, Wang J-S and Solgaard O 2007 Reconfigurable optical wavelength multiplexer using a MEMS tunable blazed grating *J. Lightwave Technol.* **25** 3100–7
[12] Davis W O, Sprague R and Miller J 2008 MEMS-based pico projector display *IEEE/LEOS Int. Conf. on Optical MEMS and Nanophotonics 2008* pp 31–2
[13] Gizmo L 2010 The latest video projectors can fit inside tiny cameras or cellphones yet still produce big pictures *IEEE Spectr.* **47** 41–5
[14] Graham-Rowe D 2007 Projectors get personal *Nat. Photon.* **1** 667–79
[15] Sun J, Guo S, Wu L, Liu L, Choe S-W, Sorg S B and Xie H 2010 3D *in vivo* optical coherence tomography based on a low-voltage, large-scan-range 2D MEMS mirror *Opt. Express* **18** 12065–75
[16] Singh J, Teo J H S, Xu Y, Premachandran C S, Chen N, Kotlanka R, Olivio M and Sheppard C J R 2008 A two axes scanning SOI MEMS micromirror for endoscopic bioimaging *J. Micromech. Microeng.* **18** 025001
[17] Yalcinkaya A D, Urey H, Brown D, Montague T and Sprague R 2006 Two-axis electromagnetic microscanner for high resolution displays *J. Microelectromech. Syst.* **15** 786–94
[18] Yalcinkaya A D, Urey H and Holmstrom S 2007 NiFe plated biaxial MEMS scanner for 2D imaging *IEEE Photon. Technol. Lett.* **19** 330–2
[19] Liao C-D and Tsai J-C 2009 The evolution of MEMS display *IEEE Trans. Ind. Electron.* **56** 1057–65
[20] Sampsell J B 1994 Digital micromirror device (DMD) and its application to projection displays *J. Vac. Sci. Technol.* B **12** 3242–6
[21] Perry T S 2004 A dark-horse technology—the grating light valve—may join the competition to dethrone the CRT *IEEE Spectr.* **41** 38–41
[22] Xie H, Pan Y and Fedder G K 2003 A CMOS-MEMS mirror with curled-hinge comb-drives *J. Microelectromech. Syst.* **12** 450–7
[23] Piyawattanametha W, Patterson R P, Hah D, Toshiyoshi H and Wu M C 2005 Surface- and bulk-micromachined two-dimensional scanner driven by angular vertical comb actuators *J. Microelectromech. Syst.* **14** 1329–38
[24] Kim J, Christensen D and Lin L 2005 Monolithic 2-D scanning mirror using self-aligned angular vertical comb drives *IEEE Photon. Technol. Lett.* **17** 2307–9
[25] Lee C 2004 Design and fabrication of epitaxial silicon micromirror devices *Sensors Actuators* A **115** 581–91
[26] Lee C, Yu A, Yan L, Wang H, He H J, Zhang Q X and Lau H J 2009 Characterization of intermediate In/Ag layers of low temperature fluxless solder based wafer bonding for MEMS packaging *Sensors Actuators* A **154** 85–91
[27] Sasaki M, Fujishima M, Hane K and Miura H 2009 Simultaneous realization of stabilized temperature characteristics and low-voltage driving of micromirror using the thin-film torsion bar of tensile poly-Si *IEEE J. Sel. Top. Quantum Electron.* **15** 1455–62
[28] Gokdel Y D, Sarioglu B, Mutlu S and Yalcinkaya A D 2009 Design and fabrication of two-axis micromachined steel scanners *J. Micromech. Microeng.* **19** 075001
[29] Ji C-H, Choi M, Kim S-C, Song K-C, Bu J-U and Ma H-J 2007 Electromagnetic two-dimensional scanner using radial magnetic field *J. Microelectromech. Syst.* **16** 989–96
[30] Isikman S O, Ergeneman O, Yalcinkaya A D and Urey H 2007 Modeling and characterization of soft magnetic film actuated 2-D scanners *IEEE J. Sel. Top. Quantum Electron.* **12** 283–9
[31] Cho I J and Yoon E 2009 A low-voltage three-axis electromagnetically actuated micromirror for fine alignment among optical devices *J. Micromech. Microeng.* **19** 085007

[32] Jia K, Pal S and Xie H 2009 An electrothermal tip-tilt-piston micromirror based on folded dual S-shaped bimorphs *J. Microelectromech. Syst.* **18** 1004–15

[33] Xu Y, Singh J, Selvarantnam T and Chen N 2009 Two-axis gimbal-less electrothermal micromirror for large-angle circumferential scanning *IEEE J. Sel. Top. Quantum Electron.* **15** 1432–8

[34] Schweizer S, Cousseau P, Lammel G, Calmes S and Renaud P 2000 Two-dimensional thermally actuated optical microprojector *Sensors Actuators* A **85** 424–9

[35] Eun Y and Kim J 2009 Thermally driven torsional micromirrors using pre-bent torsion bar for large static angular displacement *J. Micromech. Microeng.* **19** 045009

[36] Kim S-J, Cho Y-H, Nam H-J and Bu J-U 2008 Piezoelectrically pushed rotational micromirrors using detached PZT actuators for wide-angle optical switch applications *J. Micromech. Microeng.* **18** 125022

[37] Yasuda Y, Akamatsu M, Tani M, Iijima T and Toshiyoshi H 2005 Piezoelectric 2D-optical micro scanners with PZT thick films *Integr. Ferroelectr.* **76** 81–91

[38] Park J-H, Akedo J and Sato H 2007 High-speed metal-based optical microscanners using stainless-steel substrate and piezoelectric thick film prepared by aerosol deposition method *Sensors Actuators* A **135** 86–91

[39] Koh K H, Kobayashi T, Hsiao F-L and Lee C 2010 Characterization of piezoelectric PZT beam actuators for driving 2D scanning micromirror *Sensors Actuators* A **162** 336–47

[40] Kobayashi T, Ichiki M, Kondou R, Nakamura K and Maeda R 2008 Fabrication of piezoelectric microcantilevers using $LaNiO_3$ buffered $Pb(Zr,Ti)O_3$ thin film *J. Micromech. Microeng.* **18** 035007

[41] Lee C, Kawano S, Itoh T and Suga T 1996 Characteristics of sol–gel derived PZT thin films with lead oxide cover layers and lead titanate interlayers *J. Mater. Sci.* **31** 4559–68